The International Journal of Advanced Manufacturing Technology (2024) 134:1947–1964
https://doi.org/10.1007/s00170-024-14228-w

ORIGINAL ARTICLE

Gap bridging in laser welding of EN AW 5083 with different joint configurations via beam oscillation and filler wire

Kenan Kaan Yetil[1] · Daniele Colombo[2] · Yusuf Ayan[3] · Ali Gökhan Demir[1]

Received: 20 April 2024 / Accepted: 30 July 2024 / Published online: 12 August 2024

Abstract
The extended use of laser welding in the industry requires a less sensitive process in terms of geometrical tolerances of the joint edges. As the industrial availability of laser systems increases, the demand to use laser welding technology possibly with parts coming from less precise production steps is increasing. Gap formation is often caused by the edge quality of the parts coming from previous manufacturing steps such as sheet forming. Al alloy sheets deformed to box-shaped 3D forms often require welded joints on the edges in lap, but, and corner joint configurations. These joints are hard to carry out by laser welding due to the large gap formation caused by the tolerances of the deformation processes involved. Laser welding of Al alloys is already challenging in the absence of gap formation, while these joint configurations have been not feasible with a stationary beam due to incomplete fusion and defect formation. Laser welding with beam oscillation and wire feeding can improve the weldability of these joints. The oscillating motion of the high-intensity beam can achieve a deep weld together with a wider seam. Combined with wire feeding, the process can close gaps in the butt, lap, and corner joint configurations. On the other hand, the added oscillation and wire-related parameters require extending the experimental space, which requires a methodological study to identify feasible conditions. Accordingly, this work proposes a methodological approach to identify and set laser welding process parameters with beam oscillation and wire feeding for an EN AW 5083. Process parameters were initially studied using a simple analytical model that depicts the beam trajectory. Bead-on-plate tests were conducted to assess beam size, power, and weld speed ranges. Lap, butt, and corner joint conditions with a 0.5-mm gap were welded with high quality by manipulating the laser power, oscillation amplitude, and wire feed rate. The results show that welding speeds could be maintained as high as 55 mm/s with complete filling of gaps of up to 0.5 mm, eliminating the surface undercuts and achieving weld widths in the order of 2.5 mm. Moreover the results show the possibility control the depth of the welds from 3 mm to full-penetration conditions.

Keywords Wobbling · Gap formation · Keyhole welding · Robotic welding

1 Introduction

The use of laser welding in the industry is increasing as the number of welded joints increases, and the cost of ownership for laser systems decays [1]. The need for automation and the decrease in skilled labor in the welding industry also increase the need for laser welding in modern industries such as light construction [2], packaging [3], and e-mobility [4]. Such applications often make use of raw materials or semi-finished parts with scarce tolerances. Often these tolerances generate gap formation in the interface [5]. Laser welding operations with gaps in the order of the beam size have been the limitation of the process [6]. With thicknesses exceeding 1 mm, the gap value becomes more critical. The need for a less sensitive laser welding process is also followed by the increased demand for aluminum alloy welded structures [7]. Thanks to its high strength-to-low weight ratio [8], welded Al alloy structures are widely used in automotive [9], shipbuilding [10], aerospace [11], and energy industries [12]. While these industries often provide the necessary part tolerances to provide gap control, they also welcome a less

✉ Ali Gökhan Demir
aligokhan.demir@polimi.it

[1] Department of Mechanical Engineering, Politecnico di Milano, Via La Masa 1, 20156 Milan, Italy

[2] BLM Group Adige Spa, Via Per Barco 11, 38056 Levico Terme, Italy

[3] Department of Mechatronics Engineering, Karabük University, Demir Çelik Kampüsü, 78050 Karabük, Turkey

restrictive welding process in terms of tolerances [13]. The use of beam oscillation and wire feeding can provide the means for more robust and less gap-sensitive processes.

Laser welding of Al alloys poses several challenges [14]. Al alloys have high reflectivity to the commonly employed 1 μm wavelength of the solid-state lasers [15]. It has low melting and vaporizing points and a small gap between them [16]. Keyhole welding is generated via a high-intensity beam that also increases the optical absorptivity by multiple reflections [17, 18], generating a highly non-linear and unstable process. In addition to the keyhole instabilities leading to porosity [19], Al has high solubility to hydrogen in the molten phase [20] which increases the probability of pore formation. Different beam-shaping technologies have been proposed in the literature to tackle quality issues in laser welding [21, 22]. Laser beam oscillation welding has been found to be a valid option for a more stable process for Al alloys [7]. The laser beam oscillates in a chosen pattern (circular, linear, etc.), which is superimposed on the translational movement of the laser head across the workpiece [23]. Such a solution can improve the gap-bridging capability along with a reduction of the pores [24].

The application of laser welding with beam oscillation has attracted attention from both academia and industry in recent years [12]. Moreover, oscillating lasers have been used to join different materials including thermoplastic composites and metals [25]. In previous research, Al alloys of different thicknesses and grades were joined using oscillation in laser welding. In these studies, generally, the effect of the oscillation process on the microstructure and mechanical properties of welded joints was examined. Li et al. [7] performed laser welding processes on 4 mm thick AA5083 by applying oscillation at different oscillatory diameters and frequencies. In a similar study, Zhou et al. [26] combined a 2-mm thick 2060 Al–Li alloy with laser welding under different beam oscillation modes. Wang et al. [12] carried out oscillatory laser welding on 8 mm thick 5A06 aluminum alloy plates using three oscillation modes including linear, circular, and infinity modes. On the other hand, Wang et al. [27] performed laser welding by applying transverse, longitudinal, and circular mode oscillation to a 4-mm thick AA6061-T6 plate and reported that the circular mode showed the best performance. Cai et al. [28] joined 5A06-H112 Al alloys by oscillating laser welding and improved microhardness and tensile strength by achieving a finer grain structure in the oscillated joints. Ai et al. [29] investigated the effect of laser oscillation parameters on energy dissipation and dynamic behavior in T laser welding of Al alloy. They noted that oscillation parameters can modify keyhole stability, temperature distributions, flow rates, and morphologies of the molten pool.

In addition to oscillating beam applications, the use of filler wire in laser welding has a high potential to improve joint quality. Laser welding with filler wire balances focusing heat input reduces weld distortion and provides high-quality joints. Besides, the addition of filler metal provides high efficiency and can also reduce gap tolerance, improve gap bridging ability, reduce weld defects, and improve joint performance [30]. It has been stated that the use of appropriate filler wire can reduce the hot cracking susceptibility phenomenon that can be seen in Al alloys [31]. In a study, 6A02 Al alloy plates were joined by laser welding using filler wire, and a finer-grained microstructure was obtained at certain filler wire-feeding speeds compared to low speed [32]. The type of filler wire used in the laser welding process influences pore formation and joint strength as in the oscillating beam applications. Yan et al. [33] joined the AA6061-T6 alloy by laser welding using two different wires namely, ER4043 and ER5356. Researchers observed more microporosity, smaller grain size, and higher dislocation density in the joints obtained with ER4043. In addition, the tensile strength of the ER4043 joint increased by approximately 19% compared to ER5356. Except for wire feeding, the use of reinforcing material during welding was found to improve the welding performance. Xu et al. [34] joined 2A12 Al alloy with carbon nanotube reinforcement by laser welding. Due to the increased laser absorption in the alloy, they reduced the energy consumption by 33% and increased the joint strength up to 101 MPa. Appropriate determination of laser welding process parameters is also critical to obtain joints with little or no defects. Parameter optimization is required since the materials to be welded have specific properties [35]. Improper welding process adversely affects the performance of the welded joint by causing cracks, large pores, and loss of alloying elements [33]. Furthermore, the welding parameters affect the mechanical properties of the joint [36]. The chemical composition of the Al alloy grades [37] and the shielding gas content [38] used during the welding process also play an important role in the porosity of the joints.

There are significant benefits of oscillation and wire feed assistance in laser welding. The different benefits of this combination can be explored in further studies. Alloys such as AA7075 are difficult to weld due to their susceptibility to cracking. Sokoluk et al. [39] studied the welding of AA7075 alloy with TiC nanoparticle reinforced wire and showed that the joint quality can be improved by modifying the microstructure in this way. In laser welding, appropriate oscillation and wire feed parameters have the potential to stabilize the microstructure. With appropriate laser welding process parameters, it is probable that Al alloys, which are difficult to weld, can be joined by oscillation and wire feed due to the weld pool modification.

The use of beam oscillation and filler wire indeed provides several opportunities to weld less precise parts with scarce tolerances by gap bridging. However, with

an increased number of parameters the process requires a methodological approach to assess the process feasibility, reducing the number of experiments where and when possible. A certain difficulty regarding experimental studies is related to the shifting of the feasible parameter ranges concerning different weld joint types and gaps. For this reason, the construction of experimental plans in feasible ranges is an issue on its own. In the literature, studies on the effects of oscillating and wire-fed aluminum laser welding parameters on the weld seam are limited. In addition, the effects of process parameters on different Al alloy joint configurations were not widely studied. Therefore, there is a gap in the literature on these points. Accordingly, this work proposes the use of analytical modeling and sequential experimental analysis to test different process parameter ranges for different weld conditions. In particular, laser welding of EN AW 5083 plates with EN AW 5356 filler wire was investigated. Process parameter ranges were studied starting from an analytical model calculating the beam trajectory and overlap in space, later moving to bead-on-plate analyses. Finally, butt, lap, and corner joints with 0.5-mm gaps were welded employing beam oscillation and wire feeding.

2 Analytical modeling of the beam path

The use of beam oscillation in laser welding combines the high intensity of a relatively small beam (i.e. in the range of 250–350 µm diameter) with a wide seam width (i.e. in the range of 2–3 mm). Employing wide laser beams with the same power level does not necessarily provide the same penetration depth due to the reduced beam intensity [40]. For highly reflective Al alloys, the use of smaller beams is imperative to maintain a stable keyhole with a solid state operating at 1 µm wavelength [41]. If the oscillation parameters are determined appropriately, a stable melt pool can be produced with high penetration depth and width [42]. Essentially, this is provided by a keyhole that is constantly oscillating around a determined trajectory. While the depth is provided by the keyhole formation [43], the width is provided with a melt pool width in the proximity of the oscillation amplitude [44] constantly open on the material surface. The use of wire feeding is exploited to feed the missing material in the gap region [45]. In the presence of the wire, the beam oscillation also provides a further advantage in scanning over the base materials and the filler wire throughout its oscillation period. Moreover, the beam oscillation can provide an advantage of degassing with multiple passes over the same point over its trajectory.

To correctly demonstrate the feasibility of beam oscillation use, three of the most commonly used joint types in the industry, namely, butt joint, corner joint, and lap joint were investigated in the present study. Considering the additional parameters coming from the beam oscillation (i.e. oscillation frequency and amplitude), a bead-on-plate weld investigation was performed for rapid parameter determination.

Figure 1 depicts the joint configurations, material thicknesses, and approximate positions of the filling wire and laser-oscillated beam. In this context, butt welds were realized on plates with a thickness of 3 mm, and corner and lap were realized on plates with thicknesses of 3 mm and 5 mm. As can be seen, controlled varying gaps were introduced to the configurations to evaluate the bridging ability. As for the beam oscillation, circular wobbling was chosen

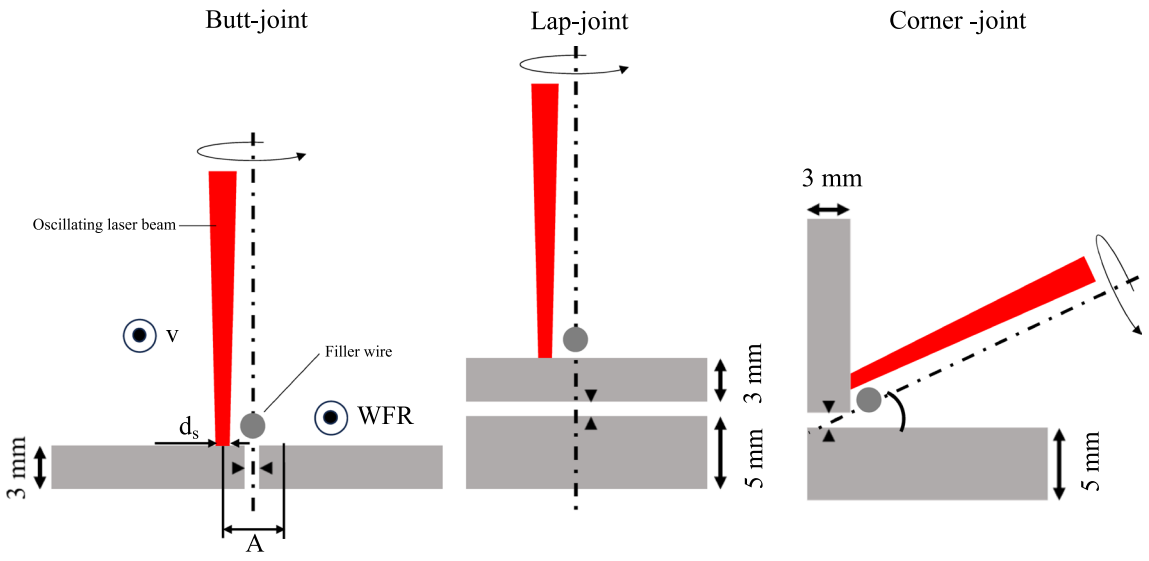

Fig. 1 Schematic description of the investigated joint configurations in the experimental work. The beam oscillation is depicted with the axis of rotation and the position of the beam on the surfaces

to be investigated. With circular wobbling, the weld seam is better shielded from undesirable atmospheric gases and homogeneity is ensured [27]. In this context, the space and velocity profiles of the wobbling beam were utilized to be able to decide the oscillation parameters.

Figure 2 demonstrates the movement of the laser beam onto the material surface. As can be seen, during the welding of the sample, there are 2 different movements that can be demonstrated; the first one is the oscillation of the laser beam, Fig. 2a, and the second one is the traverse displacement of the beam in the welding direction, Fig. 2b. The oscillation beam trajectory can be expressed using the following equations:

$$Y_{\text{travel}} = \frac{A}{2} sin(2\pi ft); X_{\text{travel}} = \frac{A}{2} cos(2\pi ft) \quad (1)$$

where A is the oscillation amplitude, f is the oscillation frequency, and t is time while the position change in the weld direction is

$$X_{weld} = v \cdot t \quad (2)$$

where v is the weld speed. As seen in Fig. 2c the two motions can be superposed. The resultant velocity components of the oscillatory motion can be expressed as follows:

$$v_{Y\text{travel}} = \frac{A}{2}(2\pi f) cos(2\pi ft); v_{X\text{travel}} = -\frac{A}{2}(2\pi f) sin(2\pi ft) \quad (3)$$

The combined beam speed can be calculated for each time instance according to the following equation.

$$v_{\text{beam}} = \sqrt{\left(v_{X\text{travel}} + v\right)^2 + \left(v_{Y\text{travel}}\right)^2} \quad (4)$$

Figure 3 schematizes the temporal variation of the velocity components of the oscillatory motion and the feed in the welding direction. As shown in Fig. 3c the velocity of the beam oscillates reaching a local minimum when the oscillatory and weld feed motion are against each other. Due to the dependence of v_{beam} to v, oscillation frequency and weld speed must be arranged properly.

Along with the speed variation, during beam oscillation, the overlapping of the beam on the weld trajectory should be also considered. Figure 4 depicts one period of a circular oscillation combined with weld speed and spot diameter. The displacement between the positions of the beam at the beginning and the end of a period equals the weld length at one period, $L_{\text{weld,1}}$, and it can be formulized by simply multiplying the time elapsing in one period, and the weld speed v as seen in the following equation.

$$L_{\text{weld,1}} = \frac{1}{f} v \quad (5)$$

An overlap equation can be derived by defining the distance of the beam at the end of a period with respect to its initial position with the following expression.

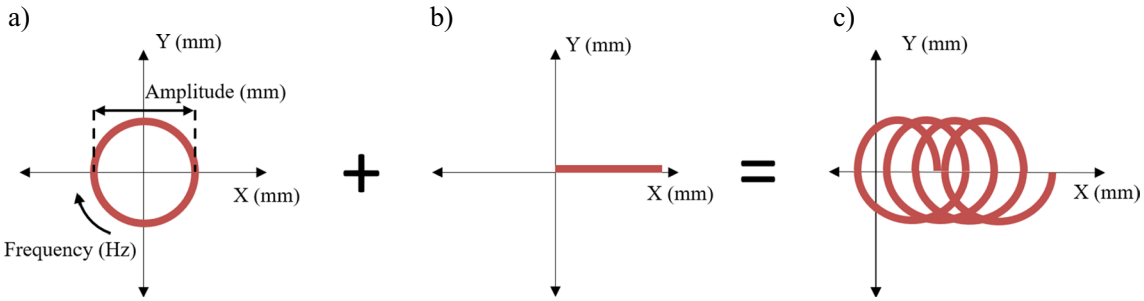

Fig. 2 **a** Wobbling beam; **b** traverse movement of the beam; and **c** superposition position of the beam movement

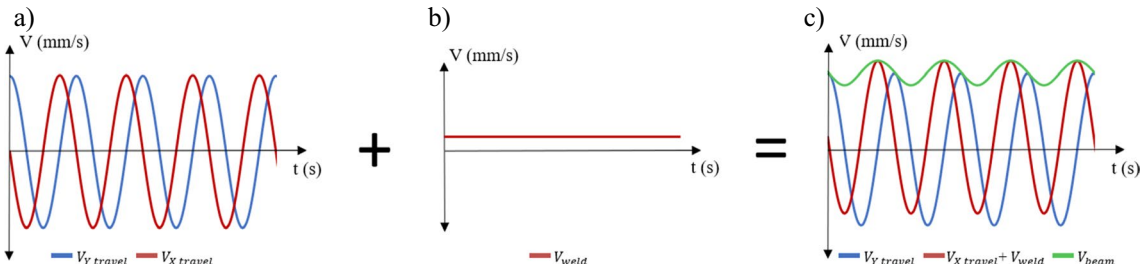

Fig. 3 **a** X and y components of the speed of the wobbling beam; **b** weld speed; and **c** superposed velocity components

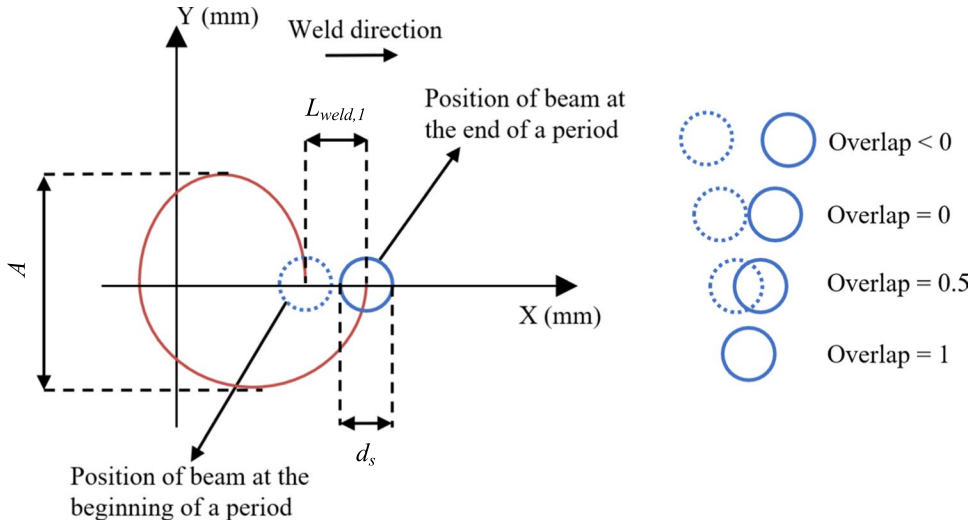

Fig. 4 Demonstrative case of one period of a circular oscillation superposed with weld speed

$$O = 1 - \frac{v}{f \cdot d_s} \tag{6}$$

where d_s is the beam spot size on the surface. According to the formula, a complete overlap equals 1 (i.e. $v = 0$), and 0 overlap is the case where the positions of the beam at the beginning and the end of a period are tangential to each other, as seen in Fig. 4.

Table 1 demonstrates the first 3 periods of an oscillating beam with different oscillation frequencies and amplitudes and having the beam diameter and weld speed fixed at 294 µm and 50 mm/s, respectively. The calculated trajectories also schematically show the extent of the beam size on the surface. With the same frequency, a larger amplitude corresponds to a higher beam speed, which can also reduce the penetration into the material. With a combination of low frequency and high amplitude, keyhole separation, and an uneven weld seam can be expected. As it can be seen, even with small amplitude values, the mismatch between the oscillation frequency and weld speed might yield an

Table 1 Laser beam trajectory during welding considering a beam diameter of 294 µm, weld speed of 50 mm/s, and different overlaps

	f = 50 Hz (O=-240%)	f = 70 Hz (O=-143%)	f = 90 Hz (O=-88%)
A = 1 mm	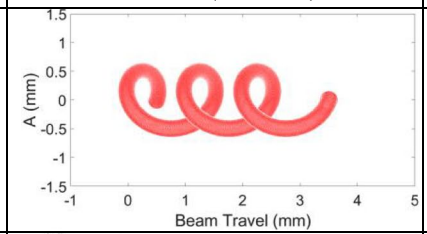	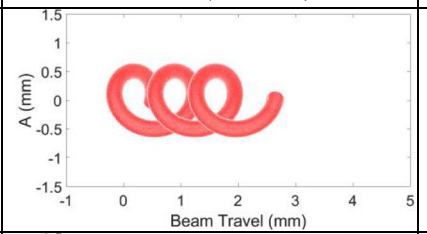	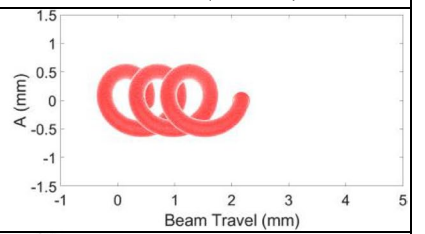
A = 1.5 mm	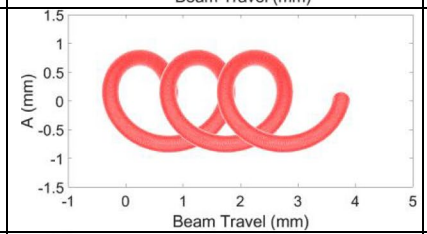	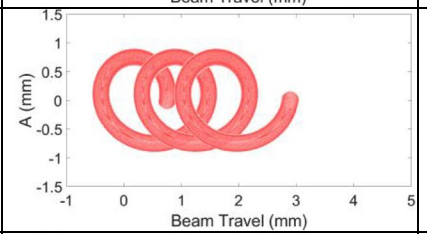	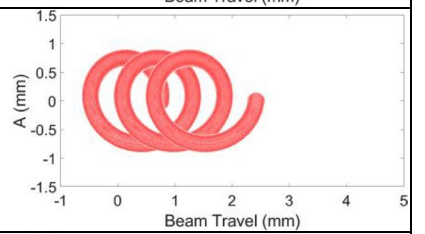
A = 2 mm	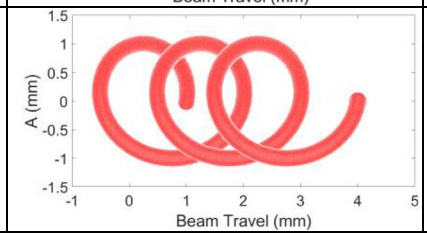	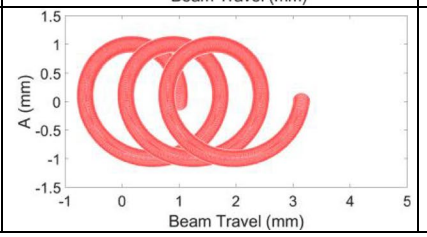	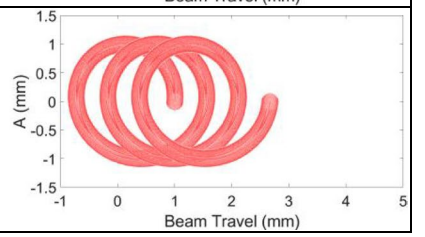

uneven laser energy distribution upon the material bringing the possibility of having an uneven melting action. For the experimental studies, the use of 70 Hz with variable oscillation amplitude was found to be adequate for weld speeds in the range of 35–85 mm/s. The overlap parameter in this range varies between − 70 and − 312% with the smallest spot size considered at 294 µm and varies between 35 and − 57% with the smallest spot size considered at 775 µm. While the modeling approach provides an overall guideline for the matching of the weld speed, beam oscillation, and oscillation amplitude, it does not consider the real seam width that is related to the beam size, power, wire-feeding parameters, and material dimensions. Because it is not possible to establish a constant relationship between the combination of all these parameters, whose effects may vary depending on the process, considering that laser welding is quite dynamic. However, the presented model provided an important guide for experimental studies in the determination of oscillation parameters.

3 Experimental system

3.1 Laser welding system

In this study, a robotic laser welding unit (BLM Adige Alphetta) was utilized consisting of a 6-degree-of-freedom robotic arm and a 2-degree-of-freedom rotary/tilting table equipped with a 6 kW multimode active fiber laser source (IPG YLP 6000) as seen in Fig. 5. As seen in Table 2, a feeding fiber with a core diameter of 100 µm was used in conjunction with a × 1.5 magnification, resulting in a focused spot size of 150 µm. The use of this robotic laser welding unit facilitates the automation of the welding processes, which proved to be more repeatable and precise. The laser beam was manipulated by means of a wobblehead (IPG D50). The device utilizes galvanometric mirrors to produce oscillating tailored shapes with a maximum frequency of 500 Hz and a maximum amplitude of 3 mm or wider for smaller oscillation frequencies. To bridge large gaps, a wire-feeding solution was utilized in the study. A wire feeder was implemented to bridge the gaps and provide the capability of feeding different wire materials at high speeds of up to 167 mm/s and with diameters up to 1.6 mm (Abicor Binzel MFS-V3). Figure 6 shows the details of the integrated

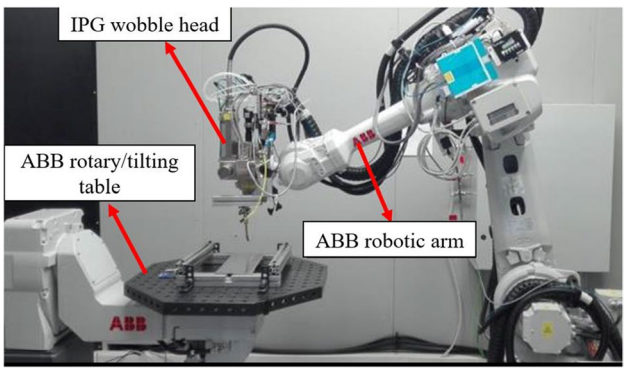

Fig. 5 Robotic welding unit equipped with the wobbling head

Table 2 Main specifications of the laser system

Parameter	Value
Wavelength, λ (nm)	1070
Available laser power, P (W)	6000
Feeding fiber core diameter, d_f (µm)	100
Focal length, f_f (mm)	300
Collimation length, f_c (mm)	200
Beam waist diameter, d_0 (µm)	150

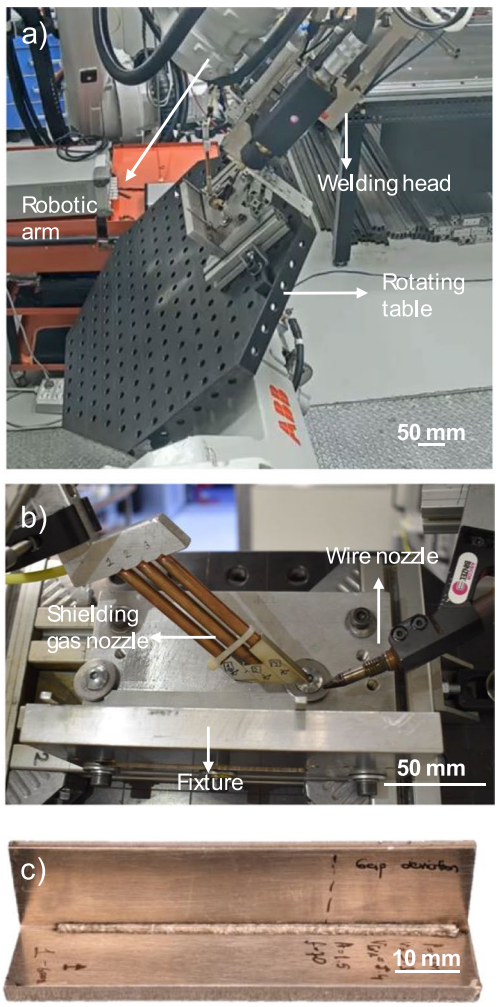

Fig. 6 Details of the experimental setup showing **a** welding configuration during a corner-joint weld, **b** the gas and wire nozzle arrangements on the fixture, and **c** macro image of a corner-joint weld

system, the nozzle configurations during an example case of corner-joint welding, and a representative image of a corner-joint weld. The test conditions for welding processes were determined as a result of plot studies based on the parameters applied in the literature for the joining of similar materials.

3.2 Materials

The material used in this study was chosen as EN AW 5083 since it has excellent corrosion resistance and weldability as well as good strength [46]. Moreover, it has a high strength-to-weight ratio and is able to maintain its strength at high temperatures. This makes it desirable for aerospace, automotive, marine, and construction industries [47]. As for the feeding wire, EN AW 5356 with a 1.1-mm diameter was chosen as it contains a relatively high amount of magnesium that brings high fluidity which makes it suitable for use as a filler wire in welding applications. By using EN AW 5083 as the base material and EN AW 5356 as the filler wire, the finished weld will retain the high strength and corrosion resistance of the base material while still having good weldability that allows the material to be joined seamlessly. Elemental contents of the materials used are given in Table 3. As seen in the table, having similar chemical compositions also helps keep the welding efficiency stable which makes them a well-suited pair.

The specimens subjected to the laser welding process were taken from 3-mm and 5-mm thick 1000 mm × 2000 mm EN AW 5083 sheets with dimensions of 100 mm × 150 mm by laser cutting machine. Before the welding process, the surfaces of these specimens were sanded and cleaned from contaminants such as oil and dirt using acetone and alcohol. Welding processes were performed with an ambient temperature of 22 °C and 50% humidity.

Table 3 Elemental content of materials used in wt%

Material	Al	Mn	Mg	Cr
EN AW 5083	Bal	0.7	4.4	0.15
EN AW 5356	Bal	0.12	5	0.12

3.3 Characterization equipment

In this study, characterization was mainly achieved by means of metallographic analysis. Cross-sectional samples were taken from the welded samples by a wire-cut electrical discharge machine (WC-EDM). The specimens were ground with SiC paper up to 600 grits [48]. Polishing processes utilized 3µ and 1µ diamond paste, respectively. To reveal the weld regions in the cross sections, Keller's reagent (95% H_2O + 2.5% HNO_3 + 1.5% HCl + 1.0% HF) was utilized. Finally, the etched samples were examined using optical microscopy (Mitutoyo Quick Vision Pro).

Figure 7 schematically describes the measurements taken at the cross-sections of the weld seams. For each joint condition, the weld width (w) at the top and the penetration depth (h) were measured as the main indicators [49]. For the joints that are not in full penetration, the depth was measured from the end tip of the weld root. For fully penetrated welds, the extent of the weld beyond the complete thickness was also added to the measurement as the wire feeding can provide the additional material to produce reinforcement. A 2^3 full factorial design with two central points was implemented and analyzed using a software package (Minitab 17). Analysis of variance (ANOVA) was applied to these measurements to assess the statistical significance of the process parameters and their interactions as well as possible curvature of the responses evaluated with the central point. An alpha value of 5% was considered for statistical significance after verifying all the hypotheses. The models were reduced to fewer interactions where required.

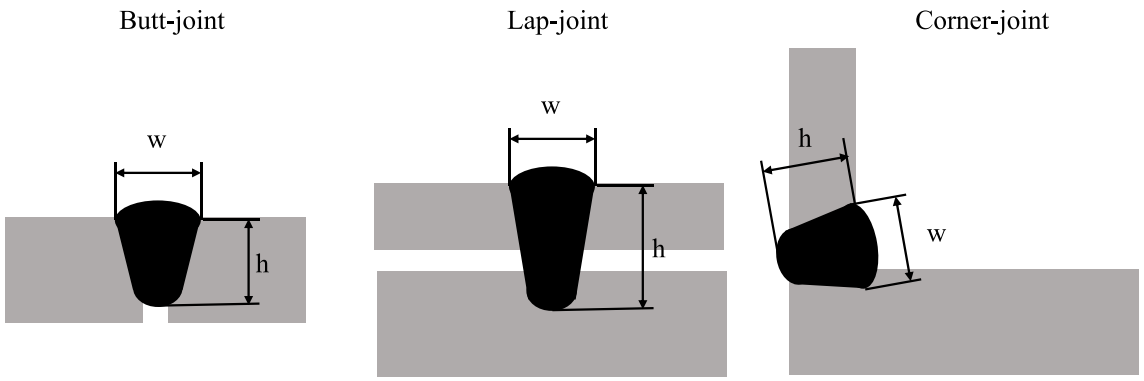

Fig. 7 The measurement of the main geometrical attributes, weld width (w), and weld depth (h) schematically shown for each weld joint type

4 Experimental investigation of beam oscillation parameters for gap bridging

4.1 Choice of the beam size

In the modeling phase, the trajectory of the laser beam is calculated in a straightforward manner. However, the calculations imply that the laser beam size approximates the weld seam size. On the other hand, a larger beam generates a reduced peak intensity. Although a larger beam may generate a denser scan path on the surface, it may also result in an insufficient penetration depth. The welding parameters used for beam size choice are given in Table 4. Considering the beam size conditions, an oscillation frequency of 70 Hz, an oscillation amplitude of 2 mm, and a welding speed of 35 mm/s were selected, which provides relatively high overlap. In order to allow for full penetration on 3 mm plates, 4 kW laser power was employed. Laser beam size was varied by defocusing at − 2.5, − 5, and − 7.5 mm producing 294 µm, 528 µm, and 775 µm beam sizes, respectively. Smaller beam sizes were avoided as they can potentially cause excessive undercuts on the upper surfaces. Wider beams were not used to avoid excessive intensity reduction. Homogenous weld seams with reduced difference between the top and bottom widths, hence reduced taper was sought.

Table 4 Fixed and variable parameters for the beam size choice

Parameters	Value
Fixed parameters	
Oscillation amplitude, *A* (mm)	2
Oscillation frequency, *f* (mm)	70
Weld speed, *v* (mm/s)	35
Laser power, *P* (kW)	4
Oscillation type	Circular
Shielding gas and flow rate (L/min)	Ar, 20
Varied parameters	
Spot size, d_s (µm)	294; 528; 775

Table 5 shows the calculated beam trajectories and the corresponding cross-section images of the produced weld seams on the plate. It can be seen that with an increase in the beam size, a denser beam path occurred as expected. This should potentially provide a homogenous and continuous melt pool. However, the cross-section image of the weld depicts a triangular seam and an incomplete penetration with $d_s = 775$ µm. The smaller beam sizes provide full penetration and reduced taper. The results show that the beam intensity should be maintained high to avoid penetration loss. In the case of $d_s = 294$ µm the cross-section images show sagging at the bottom and an undercut on the surface with a depth of approximately 1 mm, implying excessive energy in the weld seam. It can be concluded that a faster weld speed or lower laser power may be employed for a full penetration weld. In light of these results, for the successive parameter development, the spot size of laser beam was fixed at 294 µm.

4.2 Control of the weld depth on bead on plate condition

With the chosen beam size, bead-on-plate analyses were carried out to establish the variation of weld depth in stable oscillation conditions. For circular oscillation, an oscillation amplitude of 2 mm with 70 Hz frequency was found to produce a controllable weld seam shape without keyhole

Table 5 Laser beam trajectory during welding according to the parameters used in Table 4

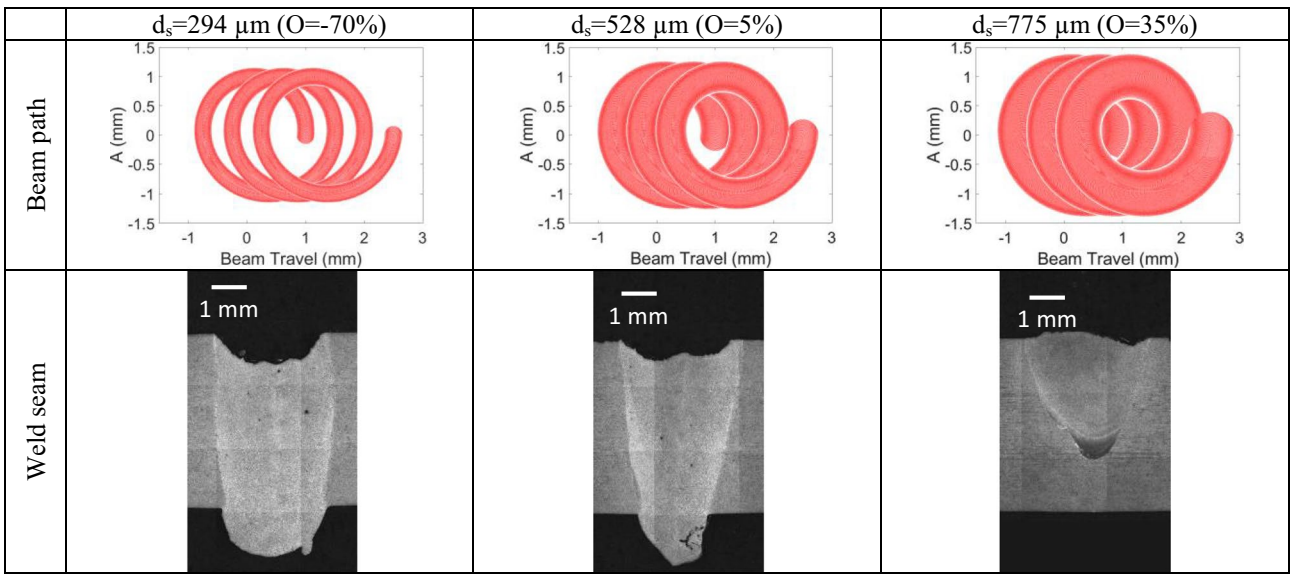

separation. Table 6 depicts the fixed and varied parameters employed in the experimental study. Laser power was varied between 3.5 and 5.5 kW, while the weld speed was varied between 55 and 85 mm/s. A full factorial plan was implemented.

Figure 8 shows the metallographic cross-section images of the experimental conditions, while Fig. 9 shows the main effects of the employed parameters on the weld seam characteristics. It can be seen that in all conditions, the weld seam is homogenous without a clear separation of the keyhole at the bottom of the seam. At high weld speeds (e.g. 85 mm/s), traces of keyhole separation are visible at the bottom side, depicting a limit overlap of the oscillation trajectory. As seen in Fig. 9, the process parameters induce little influence on the weld seam width with fixed oscillation conditions, while the weld penetration is effectively controlled between 3.5 and 5 mm. The welds' seams depict limited porosity, indicating the efficacy of the oscillation on the degassing effect.

For gap bridging in different weld conditions, it is recommended to control the weld seam width. To achieve this, the oscillation amplitude along with the laser power should be varied. On the other hand, the oscillation amplitude can be maintained fixed along with the weld speed. The wire feed rate (WFR) should be adapted to the gap width accordingly. It should be noted that the first requirement of welding in the presence of a gap is the process stability through the gap bridging. If several processing conditions may be able to provide such properties, the porosity reduction and penetration should be considered.

Table 6 Fixed and variable parameters in the bead-on-plate analysis

Parameters	Value
Fixed parameters	
Spot size, d_s (mm)	294
Oscillation amplitude, A (mm)	2
Oscillation frequency, f (mm)	70
Oscillation type	Circular
Shielding gas and flow rate (L/min)	Ar, 20
Focal position, Δz (mm)	−2.5
Varied parameters	
Laser power, P (kW)	3.5–5.5
Weld speed, v (mm/s)	55–85

4.3 Bridging of butt-joint

Table 7 shows the fixed and varied parameters in the butt-joint configuration with 3-mm plates. Considering the results of the bead-on-plate tests, a full penetration at 3 mm is expected to be found at low power conditions. A lower weld speed is also preferable to avoid keyhole separation at a fixed oscillation frequency of 70 Hz. Hence, the weld speed was fixed at 50 mm/s while the power was adjusted

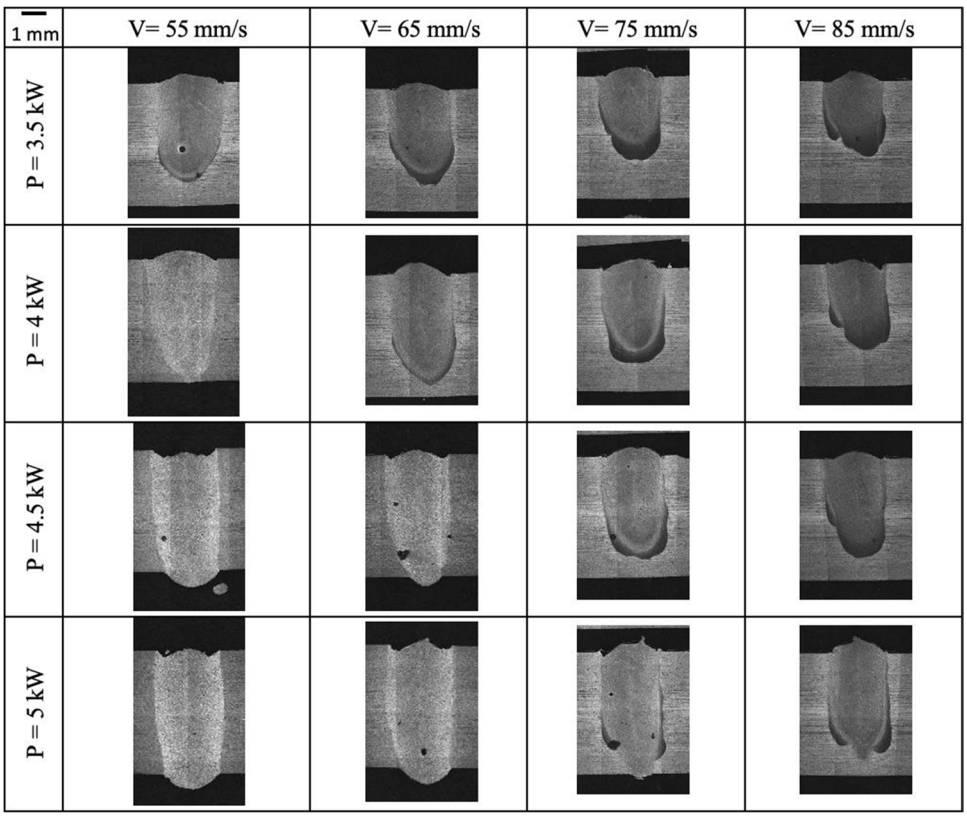

Fig. 8 The influence of laser power and weld speed at the stable oscillation conditions

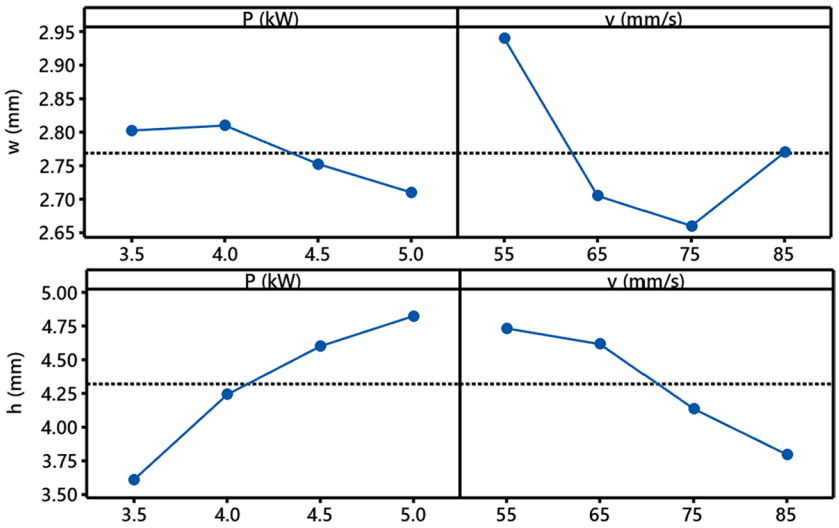

Fig. 9 Weld bead dimensions in the stable region of the bead on plate tests

between 2.25 and 3.25 kW. The missing material can be compensated via the addition of the filler wire, and a larger gap would require more wire to be added. In this respect, the WFR should be specified at different values according to the gap. The relationship between WFR, the cross-sectional area of the gap, and the cross-sectional area of the filler wire can be described by the following equation [50].

$$WFR = \frac{v.A_g}{A_w} \tag{7}$$

where WFR is the wire feed rate (mm/s), A_g is the cross-section area of gap (mm^2), v is the welding speed (mm/s), and A_w is the cross area of filler wire (mm^2). From Eq. (7), WFR was calculated as 75 mm/s. However, to deposit more material with the bottom and top of the weld, a larger WFR was considered. Hence WFR was selected between 90 and 110 mm/s.

Table 7 Fixed and variable parameters in butt-joint configuration

Parameters	Value
Fixed parameters	
Spot size, d_s (mm)	294
Weld speed, v (mm/s)	50
Oscillation type	Circular
Oscillation frequency, f (Hz)	70
Shielding gas and flow rate (l/min)	Ar, 20
Focal position, Δz (mm)	−2.5
Thickness, mm	3
Varied parameters	
Laser power, P (kW)	2.25;3.25
Oscillation amplitude, A (mm)	1.5;2
Wire feed rate, WFR (mm/s)	90;110

Figure 10 shows the resultant weld seam of butt joints as a function of the varied parameters with a gap of 0.5 mm. The images are composed to show the position of the results in the given parameter space. As seen in Fig. 9, the 2.25 kW laser power did not allow the filler wire to be deposited throughout the gap and full penetration was not achieved. At 3.25 kW, the gap bridging was better at this laser power, with a smaller oscillation amplitude and high WFR, there was excessive sagging of the weld root due to increased heat build-up. The best weld seam with sufficient reinforcement and negligible surface undercuts was achieved at 3.25 kW power, 110 mm/s WFR, and 2 mm oscillation amplitude. The coherence of these parameters together indicates a balance between the filler wire and the molten base material.

Figure 11 shows the weld width and depth as a function of the tested parameters in the butt-joint configuration. Table 8 collects the p-values of the width and depth measured from statistical analysis. For butt joint configuration only oscillation amplitude is found to be statistically significant in the case of width, while power and amplitude are statistically significant with p-values very close to the limit value (0.05). In Fig. 11, it can be seen that the weld width mainly depends on the oscillation amplitude. With larger amplitudes, larger weld widths are achieved. When the oscillation amplitude is increased, the scanning area by the laser beam expands and thus the weld pool is spread over a larger region. On the other hand, the weld depth is influenced differently by the parameters. The increase in power produces deeper welds. The total heat input increases with increasing laser power when other parameters are kept constant. Therefore, the unit energy density increases in the target region. This means that the laser beam with higher energy will penetrate the substrate more. The statistical significance of the WFR could not be confirmed. This can be expected due to the change of the material feed in the weld pool balanced by the energy

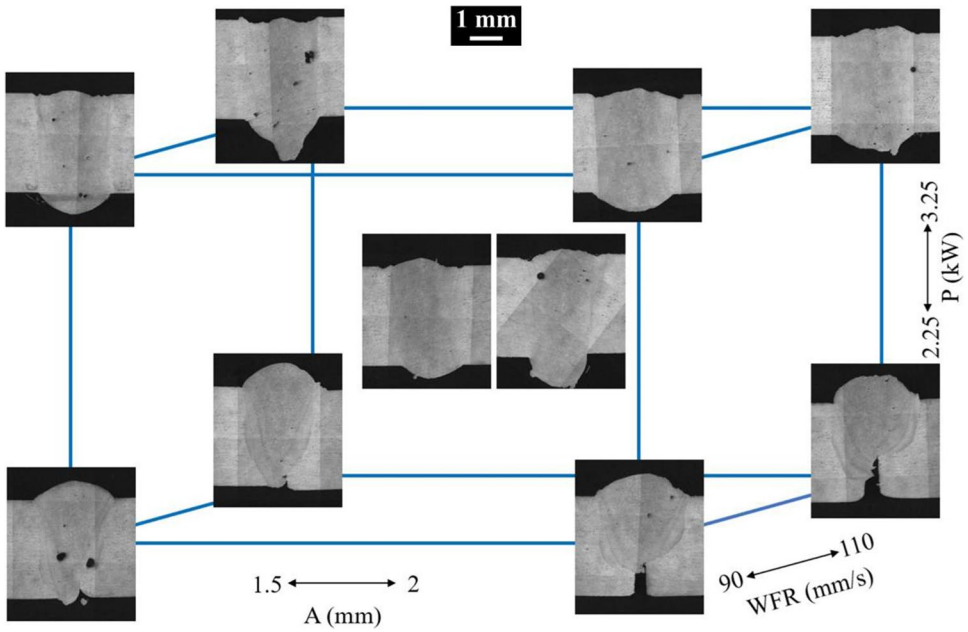

Fig. 10 The resultant conditions for bridging a 0.5-mm gap in butt-joint configuration

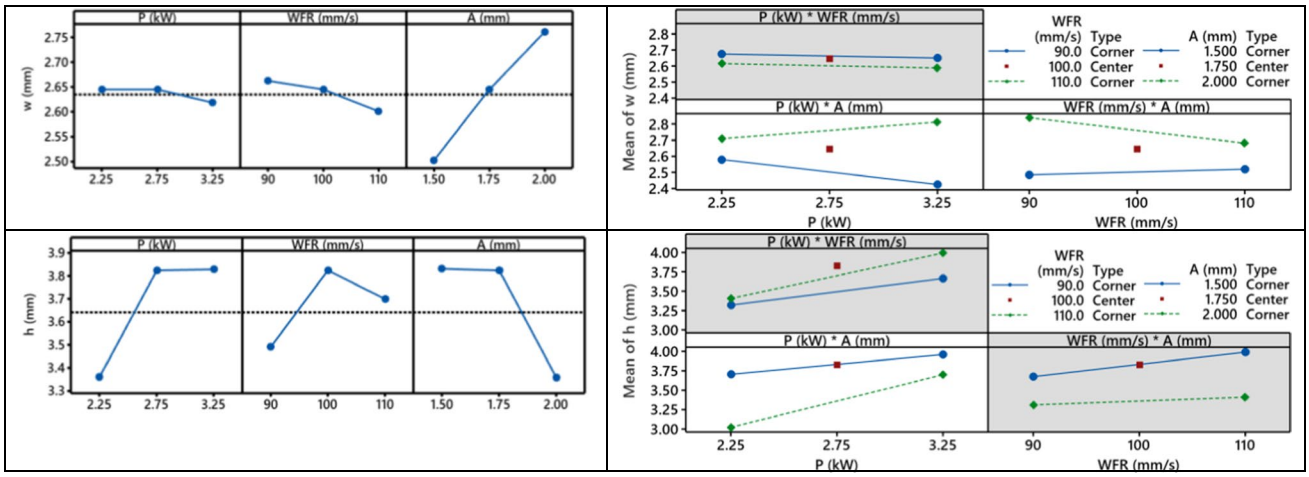

Fig. 11 Main effects and interaction plots of the weld geometry attributes in the butt-joint welds with 0.5 mm gap. Terms excluded in the final model are shaded in gray

Table 8 Combined ANOVA results for the examined conditions

	Butt-joint		Lap-joint		Corner	
Parameter	**Width**	**Depth**	**Width**	**Depth**	**Width**	**Depth**
P (kW)	0.676	*0.048*	*0.037*	*0.011*	0.735	0.106
A (mm)	*0.020*	*0.047*	*0.043*	*0.019*	*0.019*	0.618
WFR (mm/s)	0.360	0.280	0.181	0.340	0.563	0.529
P×*A*	0.108	0.270	*0.037*	0.577	-	*0.027*
P×WFR	-	-	*0.027*	0.985	0.441	0.085
A×WFR	0.189	-	0.159	0.420	*0.027*	-
Central point	0.850	0.286	0.259	0.938	0.112	0.095

The *p*-values for each measured entity are indicated. Statistically significant factors are shown in italics

input [51]. When low WFRs are combined with high power, the welds demonstrate undercuts, and the material blows away from the bottom side of the material due to induced gap-reducing depth. With higher WFRs, more material is provided in the process region reducing the risk of material blow, hence increasing depth. And further increase of WFR starts reducing the weld depth as more material must be melted. The increase of the amplitude provides a reduction effect. An increase in the amplitude increases the amount of irradiated material laterally. Hence, the depth is reduced with larger amplitudes.

4.4 Bridging of lap-joint

Lap-joint configuration poses a more difficult condition for gap bridging. The formed gap is continuous over the interface; hence, the complete filling is not a viable option. The role of the filler wire is to provide material continuity between the two layers of plates. Gap bridging of lap-joint welded Al alloys has been studied sparingly in the literature [52, 53]. A similar configuration based on lap-fillet joints has been studied, where gap bridging was achieved by the fusion of the material on the edge to provide the required material in the gap region [13, 54]. In a lap joint, the conditions may be relatively more problematic, especially in the absence of filler material. The upper sheet in the weld configuration would provide the missing material in the gap resulting in excessive undercuts and possibly deeper incisions leading to loss of weld [5]. Hence the filler wire feed should be matched to provide the missing material in the joint region. Concerning a weld width of approximately 3 mm, 0.5 mm gap, and 1.1 mm wire diameter, the ratio of WFR to the welding speed should be at least 1.5 (Eq. (7)). The total weld depth should exceed both the thickness of the first plate and the gap (i.e. > 3.5 mm). Accordingly, more powerful welding conditions are required for the considered lap joint with respect to the analyzed butt joint. Hence the power was increased and tested between 4.5 and 5.5 kW. The weld speed was fixed at 30 mm/s. The WFR was considered as 55 mm/s and 75 mm/s to provide reinforcement at the top part of the weld. The oscillation amplitude was varied between 1.5 and 2 mm. Table 9 shows the fixed and varied parameters in bridging of lap joint.

Figure 12 shows the weld seams produced using different parameter combinations in the lap-joint configuration. It can be seen that in all conditions sound welds with sufficient penetration could be achieved. All weld seams appear homogenous with limited taper. Root porosity appears to occur independently from the processing parameters. This weld defect is expected since all welds are in the partial penetration condition. Hence, degassing from the root is not possible [55]. On the other hand, beam oscillation allows to reduce the porosity extensively thanks to the generation of a larger melt pool and multiple passages of the keyhole on the molten zones [56]. Such conditions allow for a more efficient degassing and a reduced probability of gas entrapment at the keyhole root. Undercuts at the top surface appear to form at low WFR and high power possibly due to the increased surface temperature with a limited amount of material feed [57]. For improved penetration during the bridging lap joint process, the parameter combinations at 5.5 kW, 75 mm/s WFR, and 1.5 mm beam oscillation amplitude can be considered a reasonable choice with high quality.

Table 9 Fixed and variable parameters in lap-joint configuration

Parameters	Value
Fixed parameters	
Spot size, d_s (mm)	294
Weld speed, v (mm/s)	30
Oscillation frequency, f (Hz)	70
Oscillation type	Circular
Shielding gas and flow rate (L/min)	Ar, 20
Focal position, Δz (mm)	−2.5
Thickness, mm	3 on 5
Varied parameters	
Laser power, P (kW)	4.5;5.5
Oscillation amplitude, A (mm)	1.5;2
Wire feed rate, WFR (m/min)	55;75

Figure 13 shows the influence of the process parameters of the weld geometry in the lap-joint configuration. Table 8 collects the p-values of the width and depth measured on the lap-joint configuration. Laser power and amplitude as well as the interactions between them and between power and WFR are found to be statistically significant on width. Power and amplitude appear to provide a statistically significant effect on the depth. On the other hand, it can be seen that the process parameters produce limited variation in the weld width as all conditions produce similar widths at approximately 2.8 mm. The depth is increased by a higher power and a smaller amplitude corresponding to the conditions providing a higher energy input. The ability to vary the weld depth maintaining good bead quality in lap-joint configuration with gap formation demonstrates also the robustness of the approach. It can be deduced that the process can be possibly adapted to the required weld depth, but also possible power variations due to contaminations in the optical chain may still be tolerated in long production runs.

4.5 Bridging of corner joint

The corner weld condition is similar to a butt weld in terms of the required seam penetration. Full penetration is required to ensure a sound connection. The bridging of a corner weld requires the positioning of the beam with respect to

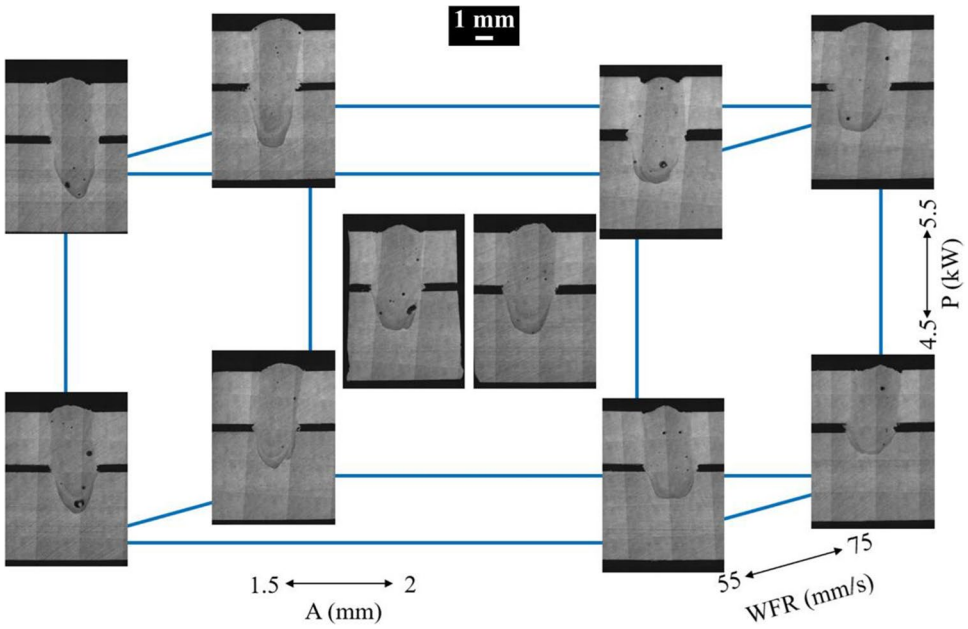

Fig. 12 The resultant conditions for bridging a 0.5-mm gap in lap-joint configuration

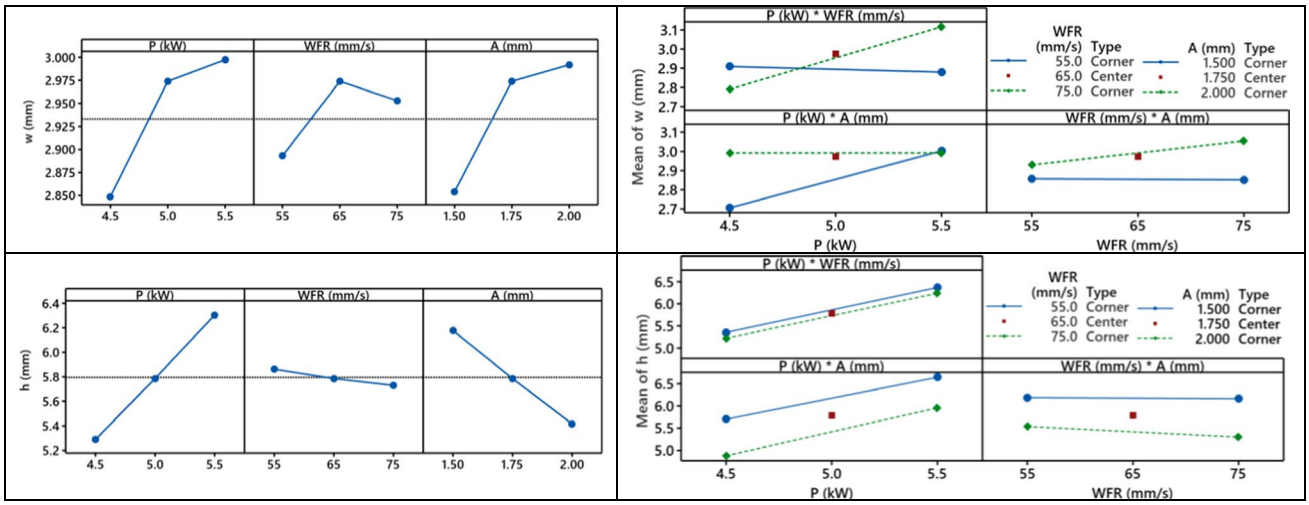

Fig. 13 Main effects and interaction plots of the weld geometry attributes in the lap-joint welds with 0.5 mm gap

the interface. If the beam is inclined more towards one of the plates, the oscillatory motion projection deviates from the ideal circular one. The inclination also elongates the welded trajectory. The smallest theoretical penetration depth is 3 mm if the beam is parallel to the horizontal plate. The feasible beam inclinations will result in a penetration depth to be higher than 3 mm. For the accessibility of the joint, the laser beam was inclined at 20° with respect to the horizontal plate. For this reason, the laser power was increased with respect to the butt-joint case to values between 3.5 and 4.5 kW. The weld speed was determined as 55 mm/s. The oscillation amplitude was varied between 1.5 and 2 mm as in the other joint configurations. In the case of the corner weld, WFR had to be increased compared to the lap-joint configuration due to the increased weld seam depth that should be compensated with the filler wire. Moreover, top reinforcement is desirable in this welding condition to avoid notching effects on the top part of the seam. Hence the WFR was varied between 110 and 130 mm/s. Table 10 shows the fixed and varied parameters in the bridging of corner joints.

Figure 14 shows the metallographic cross-sections of the obtained corner welds. It can be seen that low power results in insufficient welding towards the root of the welds. With 3.5 kW and above the weld seams penetrate thoroughly and the seam widths appear to be constant along the penetration depth. At high power, wider oscillation amplitude generates

Table 10 Fixed and variable parameters in corner-joint configuration

Parameters	Value
Fixed parameters	
Spot size, d_s (mm)	294
Weld speed, v (mm/s)	55
Oscillation frequency, f (Hz)	70
Oscillation type	Circular
Shielding gas and flow rate (L/min)	Ar, 20
Focal position, Δz (mm)	−2.5
Thickness, (mm)	3 on 5
Weld angle	20°
Varied parameters	
Laser power, P (kW)	3.5;4.5
Oscillation amplitude, A (mm)	1.5;2
Wire feed rate, WFR (mm/s)	110;130

an uneven top surface, possibly due to the wider melt flow. The central point of the experimental plan provides the most suitable compromise between sufficient penetration and a flat top surface. Figure 15 shows the effects of the process parameters in the corner-joint configuration. Table 8 collects the p-values of the width and depth measured on the corner-joint configuration. Only amplitude was found to have a statistically significant effect on the width, while the interaction between power and amplitude was found to have a statistically significant effect on the depth. The overall variation observed on the weld width at the top surface as a function of the process parameters is limited since the values are approximately 2.7 mm. On the other hand, the process parameters appear to have a more pronounced effect on the weld depth as the central point provides the highest depth varying values between 4.6 and 5.4 mm. The overall controllability of the weld depth is highly appealing to control the material reinforcement at the weld root.

5 Discussion

Different welding parameters including laser power, beam oscillation amplitude, and WFR caused various effects depending on the changing joint configurations. The effect levels of these parameters varied on weld width and weld depth according to joint types. The results showed that the oscillation amplitude had a significant effect on all three joint configurations. Increasing the oscillation amplitude expanded the weld width and decreased the weld depth in all three joints. Moreover, the rise in weld seam width provided compliance with the laser oscillation path models presented in Table 1. When the oscillation amplitude increases, the scanned area by the laser beam increases, and thus, the weld pool spreads over a larger region. This can be attributed to increased oscillation magnitude spreading the energy accumulation over a wider gap [58]. In this respect, more laser energy is absorbed in the direction of the weld width, and energy is lost in the direction of the weld depth [59]. Zhang et al. [60] reported that higher amplitude increases the speed of movement of the keyhole and the drag force, thus increasing the stirring effect produced by the keyhole. Therefore, higher amplitude results in a larger melting pool. This may disrupt the balance between surface tension pressure and recoil pressure and create a hole around the keyhole after the weld pool solidifies [24]. Thanks to the wire feeding together

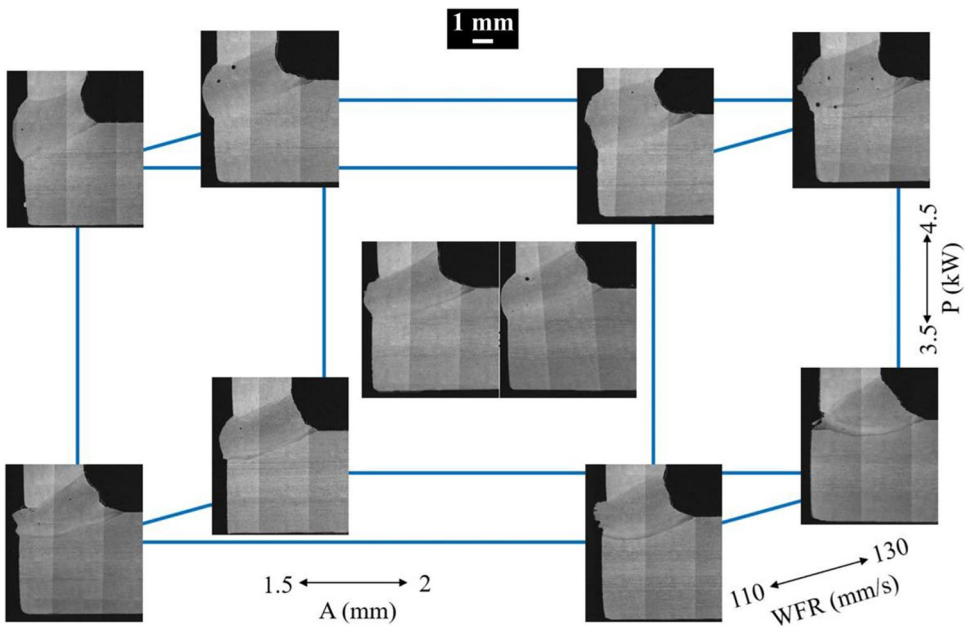

Fig. 14 The resultant conditions for bridging a 0.5-mm gap in corner-joint configuration

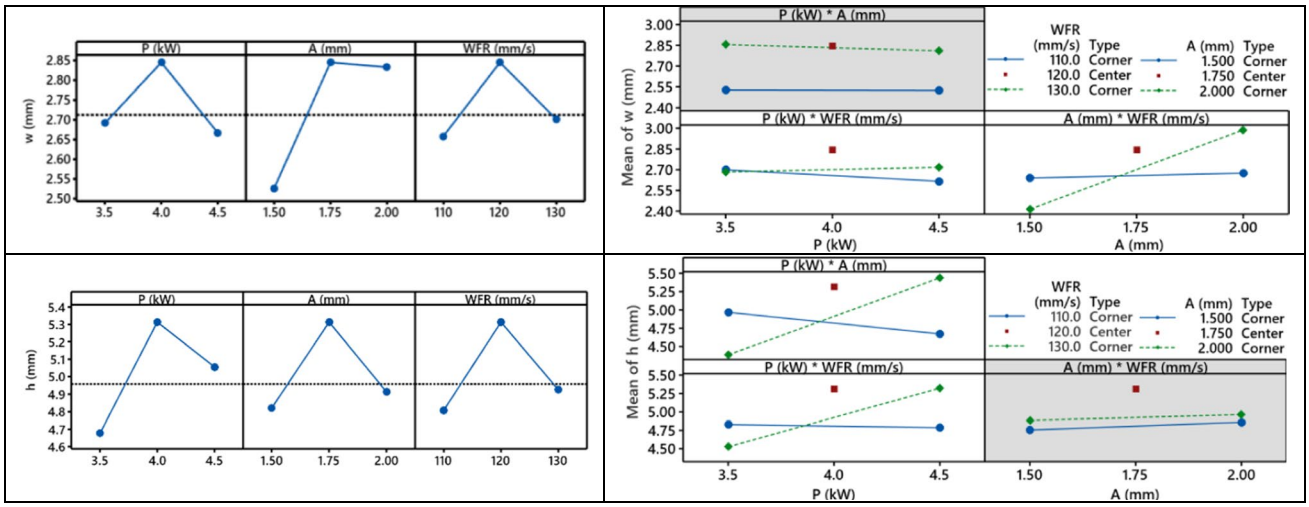

Fig. 15 Main effects and interaction plots of the weld geometry attributes in the corner welds with 0.5 mm gap. Terms excluded in the final model are shaded in gray

with the oscillation mode presented in the study, melt pool disruption was prevented by adding material in the weld pool. This demonstrates the feasibility of high amplitude in the laser welding process by using wire feed and oscillation.

Laser power is a key parameter that provides the required heat input for joining processes. Welding depth depends mainly on heat input, which varies with welding speed and laser power. When the welding speed is kept constant and the applied laser power increases, the heat input and the resulting power density will increase. Choosing the laser power above or below the required amount directly affects the formations and dimensions of the weld seam. According to the results, laser power had a significant effect on weld depth in all joint types (butt and lap) except corner weld configuration. When higher laser power was increased in butt and lap joints, welding depths increased. Similar increments were seen in butt [53] and lap joints [61] in previous studies. This can be attributed to the increase in energy per unit area on the seam. It has been mentioned that high laser power may cause some welding defects such as underfill and undercut by evaporating more metal [62]. However, the laser power could be balanced with the wire feeding utilized in the present work, and material loss could be prevented with additional wire even when using high laser power. It can be concluded that gap bridging can be performed by applying higher power in laser welding with the use of wire feeding.

WFR is another parameter that is chosen as a variable in the laser welding processes. According to the results, WFR did not show significant results on the weld width and depth for all three joint configurations. However, laser welding with filler wire includes three basic processes that affect weld stability and weld quality: wire melting and transfer behavior, keyhole and molten pool dynamics, and fluid flow in the molten pool [63]. While the WFR was not found to significantly influence the width and depth statistically, it was seen that wire feeding allowed to achieve a homogenous weld seam reducing the formation of undercuts.

6 Conclusions

This work showed a systematic analysis of laser welding parameters with beam oscillation and wire feeding for an EN 5083 Al alloy. The Al alloys that are conventionally difficult to weld with a laser beam due to their high reflectivity were successfully welded in the presence of a 0.5-mm gap in three different weld configurations thanks to the combined effect of the beam oscillation and added wire. The general outcomes of the study are as follows.

- The use of a highly intense laser beam with a relatively small spot size (i.e. 294 µm) allowed to maintain keyhole processing in all conditions providing the depth. The oscillating motion provided the means to enlarge the seam to reduce the process sensitivity to the gap presence. The added filler wire compensated for the missing material in the gap.
- The methodological approach showed that oscillation amplitude and frequency should be matched to the weld speed in order to avoid keyhole separation. The WFR should be chosen to provide the missing material in the presence of a gap, according to the cross-sectional area of the gap, the cross-sectional area of the filler wire, and the weld speed.
- The welding speeds could be maintained as high as 50, 30, and 55 mm/s with butt, lap, and corner joint configu-

rations, respectively. Complete filling of gaps of up to 0.5 mm, eliminating the surface undercuts, and achieving weld widths in the order of 2.5 mm. Moreover, the results show the possibility control the depth of the welds from 3 mm to full-penetration conditions. Surface undercuts were eliminated.

- The results show that the use of beam oscillation provided high-quality seams with moderate power levels, providing conditions that come close to 1 kW/1 mm weld depth.

The results of this work show a framework to study the process parameters to weld different configurations. Future works will deal with the combined use of thermal models to assist the parameter development to further reduce the overall experimental burden.

Author contribution Kenan Kaan Yetil: data curation, formal analysis, investigation, visualization, and writing—original draft. Daniele Colombo: conceptualization, resources, and writing—review and editing. Yusuf Ayan: data curation, formal analysis, investigation, and writing—review and editing. Ali Gökhan Demir: conceptualization, formal analysis, methodology, resources, supervision, and writing—original draft.

Funding Open access funding provided by Politecnico di Milano within the CRUI-CARE Agreement.

Declarations

Conflict of interest The authors declare no competing interests.

References

1. Belforte D (2020) Market pressures dampen 2019 results. Industrial laser solutions 35(1):9–13
2. L. Caprio, G. Borzoni, B. Previtali, and A. G. Demir, "Hand-held laser welding of AISI301LN for components with aesthetic requirements: toward the integration of machine and human intelligence," *J Laser Appl*, vol. 35, no. 1, Feb. 2023, https://doi.org/10.2351/7.0000746.
3. Shukla P (2014) Investigation into the high-speed laser welding feasibility of tin-plated steels available for three-piece food packaging can manufacture. Proc Inst Mech Eng B J Eng Manuf 228(7):715–729. https://doi.org/10.1177/0954405413498729
4. S. D'Arcangelo *et al.*, "Comprehensive benchmarking of laser welding technologies including novel beam shapes and wavelengths for e-drive copper hairpins," *Opt Laser Technol*, vol. 169, Feb. 2024, https://doi.org/10.1016/j.optlastec.2023.109964.
5. Garavaglia M, Demir AG, Zarini S, Victor BM, Previtali B (2020) Fiber laser welding of AA 5754 in the double lap-joint configuration: process development, mechanical characterization, and monitoring. The International Journal of Advanced Manufacturing Technology 111(5–6):1643–1657. https://doi.org/10.1007/s00170-020-06128-6
6. Colombo D, Colosimo BM, Previtali B (2013) Comparison of methods for data analysis in the remote monitoring of remote laser welding. Opt Lasers Eng 51(1):34–46. https://doi.org/10.1016/j.optlaseng.2012.07.022
7. Li S, Mi G, Wang C (2020) A study on laser beam oscillating welding characteristics for the 5083 aluminum alloy: morphology, microstructure and mechanical properties. J Manuf Process 53:12–20. https://doi.org/10.1016/j.jmapro.2020.01.018
8. S. G. Kang and J. Shin, "The effect of laser beam intensity distribution on weld characteristics in laser welded aluminum alloy (AA5052)," *Opt Laser Technol*, vol. 142, Oct. 2021, https://doi.org/10.1016/j.optlastec.2021.107239.
9. Hong KM, Shin YC (2017) Prospects of laser welding technology in the automotive industry: a review. J Mater Process Technol 245:46–69. https://doi.org/10.1016/j.jmatprotec.2017.02.008
10. G. Turichin, M. Kuznetsov, I. Tsibulskiy, and A. Firsova, "Hybrid Laser-arc welding of the high-strength shipbuilding steels: equipment and technology," in *Physics Procedia*, Elsevier B.V., 2017, pp. 156–163. https://doi.org/10.1016/j.phpro.2017.08.005.
11. J. Blackburn, "Laser welding of metals for aerospace and other applications."
12. Wang Z, Oliveira JP, Zeng Z, Bu X, Peng B, Shao X (2019) Laser beam oscillating welding of 5A06 aluminum alloys: microstructure, porosity and mechanical properties. Opt Laser Technol 111:58–65. https://doi.org/10.1016/j.optlastec.2018.09.036
13. P. Franciosa, A. Serino, R. Al Botros, and D. Ceglarek, "Closed-loop gap bridging control for remote laser welding of aluminum components based on first principle energy and mass balance," *J Laser Appl*, vol. 31, no. 2, p. 022416, 2019, https://doi.org/10.2351/1.5096099.
14. Katayama S, Nagayama H, Mizutani M, Kawahito Y (2009) Fibre laser welding of aluminium alloy. Weld Int 23(10):744–752. https://doi.org/10.1080/09507110902836911
15. WilliamM. Steen JyotirmoyMazumder, *Laser material processing 4th edition*. https://doi.org/10.1007/978-1-84996-062-5.
16. Zhao H, White DR, Debroy T (1999) Current issues and problems in laser welding of automotive aluminum alloys. Int Mater Rev 44(6):238–266. https://doi.org/10.1179/095066099101528298
17. J. Xu, Y. Rong, Y. Huang, P. Wang, and C. Wang, "Keyhole-induced porosity formation during laser welding," *J Mater Process Technol*, vol. 252, no. October 2017, pp. 720–727, 2018, https://doi.org/10.1016/j.jmatprotec.2017.10.038.
18. Kim H, Nam K, Kim Y, Ki H (2022) Analysis of laser-beam absorptance and keyhole behavior during laser keyhole welding of aluminum alloy using a deep-learning-based monitoring system. J Manuf Process 80(May):75–86. https://doi.org/10.1016/j.jmapro.2022.05.044
19. Xiao R, Zhang X (2014) Problems and issues in laser beam welding of aluminum–lithium alloys. J Manuf Process 16(2):166–175. https://doi.org/10.1016/j.jmapro.2013.10.005
20. Weingarten C, Buchbinder D, Pirch N, Meiners W, Wissenbach K, Poprawe R (2015) Formation and reduction of hydrogen porosity during selective laser melting of AlSi10Mg. J Mater Process Technol 221:112–120. https://doi.org/10.1016/j.jmatprotec.2015.02.013

21. Sun T, Mohan A, Liu C, Franciosa P, Ceglarek D (2022) The impact of adjustable-ring-mode (ARM) laser beam on the microstructure and mechanical performance in remote laser welding of high strength aluminium alloys. J Market Res 21:2247–2261. https://doi.org/10.1016/j.jmrt.2022.10.055
22. F. Galbusera, L. Caprio, B. Previtali, and A. G. Demir, "The influence of novel beam shapes on melt pool shape and mechanical properties of LPBF produced Al-alloy," *J Manuf Process*, vol. 85, no. September 2022, pp. 1024–1036, 2023, https://doi.org/10.1016/j.jmapro.2022.12.007.
23. Shah LH, Khodabakhshi F, Gerlich A (2019) Effect of beam wobbling on laser welding of aluminum and magnesium alloy with nickel interlayer. J Manuf Process 37:212–219. https://doi.org/10.1016/j.jmapro.2018.11.028
24. Idriss M, Mirakhorli F, Desrochers A, Maslouhi A (2022) Overlap laser welding of 5052–H36 aluminum alloy: experimental investigation of process parameters and mechanical designs. Int J Adv Manuf Technol 119(11–12):7653–7667. https://doi.org/10.1007/s00170-022-08783-3
25. S. Hu and F. Li, "Laser joining of CFRTP to metal: a review on welding parameters, joint enhancement, and numerical simulation," Feb. 20, 2024, *John Wiley and Sons Inc*. https://doi.org/10.1002/pc.27914.
26. Zhou X et al (2021) Effects of beam oscillation modes on microstructure and mechanical properties of laser welded 2060 Al-Li alloy joints. Opt Laser Technol 144:107389. https://doi.org/10.1016/j.optlastec.2021.107389
27. Wang L, Gao M, Zhang C, Zeng X (2016) Effect of beam oscillating pattern on weld characterization of laser welding of AA6061-T6 aluminum alloy. Mater Des 108:707–717. https://doi.org/10.1016/j.matdes.2016.07.053
28. J. Cai, Y. Wei, Z. Ouyang, X. Liu, H. Jin, and J. Chen, "Investigation on clockwise circular oscillating laser welding for the 5A06-H112 aluminum alloy: energy distribution, seam appearance, microstructure, and mechanical properties," *Opt Laser Technol*, vol. 176, Sep. 2024, https://doi.org/10.1016/j.optlastec.2024.111026.
29. Y. Ai, J. Liu, C. Ye, and J. Cheng, "Influence of oscillation parameters on energy distributions and dynamic behaviors during laser welding of aluminum alloy T-joints assisted with solder patch," *International Journal of Thermal Sciences*, vol. 201, Jul. 2024, https://doi.org/10.1016/j.ijthermalsci.2024.108953.
30. Zhang K, Li D, Gui H, Li Z (2018) Adaptive control for laser welding with filler wire of marine high strength steel with tight butt joints for large structures. J Manuf Process 36:434–441. https://doi.org/10.1016/j.jmapro.2018.10.042
31. Enz J, Carrarin C, Riekehr S, Ventzke V, Kashaev N (2018) Hot cracking behaviour of an autogenously laser welded Al-Cu-Li alloy. Int J Adv Manuf Technol 95(1–4):299–310. https://doi.org/10.1007/s00170-017-1197-x
32. Xu F, Chen L, He EG, Guo LY (2019) "Laser welding 6A02 aluminum alloy with filler wire under high welding speed", in *IOP conference series: materials science and engineering*. Institute of Physics Publishing. https://doi.org/10.1088/1757-899X/504/1/012028
33. Yan S, Xing B, Zhou H, Xiao Y, Qin QH, Chen H (2018) Effect of filling materials on the microstructure and properties of hybrid laser welded Al-Mg-Si alloys joints. Mater Charact 144:205–218. https://doi.org/10.1016/j.matchar.2018.07.018
34. T. Xu, Z. Zhu, G. Mi, S. L. Sing, and X. Ma, "Simultaneous reduction in laser welding energy consumption and strength improvement of aluminum alloy joint by addition of trace carbon nanotubes," *J Clean Prod*, vol. 448, Apr. 2024, https://doi.org/10.1016/j.jclepro.2024.141557.
35. Darmadi DB, Gapsari F, Dirman SR, Talice M (2023) Optimum power for ER-70S-2 AND SS400 dissimilar CDW joint. Journal of Applied Engineering Science 21(2):392–400. https://doi.org/10.5937/jaes0-39068
36. Afriansyah Z, Ashof M, Naimah A (2024) Comparison of SMAW and GTAW welding properties. Mechanics exploration and material innovation 1(2):48–53. https://doi.org/10.21776/ub.memi.2024.001.02.2
37. Huang L, Hua X, Wu D, Fang L, Cai Y, Ye Y (2018) Effect of magnesium content on keyhole-induced porosity formation and distribution in aluminum alloys laser welding. J Manuf Process 33:43–53. https://doi.org/10.1016/j.jmapro.2018.04.023
38. Vyskoč M, Sahul M, Sahul M (2018) Effect of shielding gas on the properties of AW 5083 aluminum alloy laser weld joints. J Mater Eng Perform 27(6):2993–3006. https://doi.org/10.1007/s11665-018-3383-x
39. M. Sokoluk, C. Cao, S. Pan, and X. Li, "Nanoparticle-enabled phase control for arc welding of unweldable aluminum alloy 7075," *Nat Commun*, vol. 10, no. 1, Dec. 2019, https://doi.org/10.1038/s41467-018-07989-y.
40. Kaymak Y, Rojas-Cessa R, Feng J, Ansari N, Zhou M (2017) On divergence-angle efficiency of a laser beam in free-space optical communications for high-speed trains. IEEE Trans Veh Technol 66(9):7677–7687. https://doi.org/10.1109/TVT.2017.2686818
41. Y. M. Baqer *et al.*, "Fiber laser welding of similar and dissimilar aluminum alloys," 2021.
42. Li J, Sun Q, Liu Y, Zhen Z, Sun Q, Feng J (2020) Melt flow and microstructural characteristics in beam oscillation superimposed laser welding of 304 stainless steel. J Manuf Process 50:629–637. https://doi.org/10.1016/j.jmapro.2019.12.053
43. Jin X, Li L (2004) An experimental study on the keyhole shapes in laser deep penetration welding. Opt Lasers Eng 41(5):779–790. https://doi.org/10.1016/S0143-8166(03)00034-4
44. M. Jarwitz, F. Fetzer, R. Weber, and T. Graf, "Weld seam geometry and electrical resistance of laser-welded, aluminum-copper dissimilar joints produced with spatial beam oscillation," *Metals (Basel)*, vol. 8, no. 7, Jul. 2018, https://doi.org/10.3390/met8070510.
45. S. Zhang, J. Sun, M. Zhu, L. Zhang, P. Nie, and Z. Li, "Fiber laser welding of HSLA steel by autogenous laser welding and autogenous laser welding with cold wire methods," *J Mater Process Technol*, vol. 275, Jan. 2020, https://doi.org/10.1016/j.jmatprotec.2019.116353.
46. R. Bauri, D. Yadav, C. N. Shyam Kumar, and B. Balaji, "Tungsten particle reinforced Al 5083 composite with high strength and ductility," *Materials science and engineering: A*, vol. 620, pp. 67–75, Jan. 2015, https://doi.org/10.1016/j.msea.2014.09.108.
47. D. Istrate *et al.*, "Correlation between mechanical properties—structural characteristics and cavitation resistance of cast aluminum alloy type 5083," *Crystals (Basel)*, vol. 12, no. 11, Nov. 2022, https://doi.org/10.3390/cryst12111538.
48. A. K. Maurya, W. N. Khan, A. Patnaik, M. Ş. Adin, R. Chhibber, and C. Pandey, "Tribological performance of gas tungsten arc welded dissimilar joint of sDSS 2507/IN-625 for marine application," *Archives of Civil and Mechanical Engineering*, vol. 24, no. 1, Feb. 2024, https://doi.org/10.1007/s43452-023-00832-2.
49. Stavridis J, Papacharalampopoulos A, Stavropoulos P (2018) Quality assessment in laser welding: a critical review. Int J Adv Manuf Technol 94(5–8):1825–1847. https://doi.org/10.1007/s00170-017-0461-4
50. Yu YC et al (2013) Multi-pass laser welding of thick plate with filler wire by using a narrow gap joint configuration. J Mech Sci Technol 27(7):2125–2131. https://doi.org/10.1007/s12206-013-0525-9
51. Yu Y et al (2013) Investigation of melting dynamics of filler wire during wire feed laser welding. J Mech Sci Technol 27(4):1097–1108. https://doi.org/10.1007/s12206-013-0218-4

52. Woizeschke P, Vollertsen F (2020) Laser keyhole micro welding of aluminum foils to lap joints even with large gap sizes. CIRP Ann 69(1):237–240. https://doi.org/10.1016/j.cirp.2020.04.063
53. L. Chen, C. Wang, L. Xiong, X. Zhang, and G. Mi, "Microstructural, porosity and mechanical properties of lap joint laser welding for 5182 and 6061 dissimilar aluminum alloys under different place configurations," *Mater Des*, vol. 191, Jun. 2020, https://doi.org/10.1016/j.matdes.2020.108625.
54. Sharma A, Mohanty UK, Tanaka M, Suga T (2021) Mechanism of gap bridgeability in lap-fillet laser-arc hybrid welding. Lasers in manufacturing and materials processing 8(3):355–371. https://doi.org/10.1007/s40516-021-00150-6
55. Huang L, Hua X, Wu D, Ye Y (2019) Role of welding speed on keyhole-induced porosity formation based on experimental and numerical study in fiber laser welding of Al alloy. Int J Adv Manuf Technol 103(1–4):913–925. https://doi.org/10.1007/s00170-019-03502-x
56. W. Tao and S. Yang, "Weld zone porosity elimination process in remote laser welding of AA5182-O aluminum alloy lap-joints," *J Mater Process Technol*, vol. 286, Dec. 2020, https://doi.org/10.1016/j.jmatprotec.2020.116826.
57. Garavaglia M, Demir AG, Zarini S, Victor BM, Previtali B (2019) Process development and coaxial sensing in fiber laser welding of 5754 Al-alloy. J Laser Appl 31(2):022419. https://doi.org/10.2351/1.5096101
58. J. Yang, T. Li, W. Ye, J. Chen, and J. Qiao, "Effect of beam oscillation amplitude on microstructure and mechanical properties of small laser spot welded QP980 Steel," *Metals (Basel)*, vol. 13, no. 8, Aug. 2023, https://doi.org/10.3390/met13081363.
59. Y. Ai, L. Yu, Y. Huang, and X. Liu, "The investigation of molten pool dynamic behaviors during the '∞' shaped oscillating laser welding of aluminum alloy," *International Journal of Thermal Sciences*, vol. 173, Mar. 2022, https://doi.org/10.1016/j.ijthermalsci.2021.107350.
60. Zhang C, Li X, Gao M (2020) Effects of circular oscillating beam on heat transfer and melt flow of laser melting pool. J Market Res 9(4):9271–9282. https://doi.org/10.1016/j.jmrt.2020.06.030
61. Wu Z et al (2023) Effect of thermophysical properties on porosity and microstructure of laser welded cast and wrought aluminum alloy dissimilar lap joints. J Market Res 26:1833–1849. https://doi.org/10.1016/j.jmrt.2023.08.021
62. Y. Li, M. Xiong, Y. He, J. Xiong, X. Tian, and P. Mativenga, "Multi-objective optimization of laser welding process parameters: the trade-offs between energy consumption and welding quality," *Opt Laser Technol*, vol. 149, May 2022, https://doi.org/10.1016/j.optlastec.2022.107861.
63. Ma G, Li L, Chen Y (2017) Effects of beam configurations on wire melting and transfer behaviors in dual beam laser welding with filler wire. Opt Laser Technol 91:138–148. https://doi.org/10.1016/j.optlastec.2016.12.019